

Ultraviolet metalens and metalens array of focused vortex beams

Jinping Zhang(张金平), Yan Wang(王焱), Huan Yuan(袁欢), Zehao Wang(王泽豪), Yang Deng(邓阳), Chengzhi Huang(黄承志), Jiagui Wu(吴加贵), and Junbo Yang(杨俊波)

Citation: Chin. Phys. B, 2023, 32 (**6**): 064206. DOI: 10.1088/1674-1056/ac9d87
Journal homepage: http://cpb.iphy.ac.cn; http://iopscience.iop.org/cpb

What follows is a list of articles you may be interested in

Design of broadband achromatic metasurface device based on phase-change material $Ge_2Sb_2Te_5$

Shuyuan Lv(吕淑媛), Xinhui Li(李新慧), Wenfeng Luo(罗文峰), and Jie Jia(贾洁)
Chin. Phys. B, 2022, 31 (**12**): 124206. DOI: 10.1088/1674-1056/ac657a

Design of an all-dielectric long-wave infrared wide-angle metalens

Ning Zhang(张宁), Qingzhi Li(李青芝), Jun Chen(陈骏), Feng Tang(唐烽),Jingjun Wu(伍景军), Xin Ye(叶鑫), and Liming Yang(杨李茗)
Chin. Phys. B, 2022, 31 (**7**): 074212. DOI: 10.1088/1674-1056/ac4026

Temperature-responded tunable metalenses based on phase transition materials

Jing-Jun Wu(伍景军), Feng Tang(唐烽), Jun Ma(马骏), Bing Han(韩冰), Cong Wei(魏聪), Qing-Zhi Li(李青芝), Jun Chen(陈骏), Ning Zhang(张宁), Xin Ye(叶鑫), Wan-Guo Zheng(郑万国)‡, and Ri-Hong Zhu(朱日宏)
Chin. Phys. B, 2022, 31 (**5**): 054216. DOI: 10.1088/1674-1056/ac3cad

Solar energy full-spectrum perfect absorption and efficient photo-thermal generation

Zhefu Liao(廖喆夫), Zhengqi Liu(刘正奇), Qizhao Wu(吴起兆), Xiaoshan Liu(刘晓山), Xuefeng Zhan(詹学峰), Gaorong Zeng(曾高荣), and Guiqiang Liu(刘桂强)
Chin. Phys. B, 2021, 30 (**8**): 084206. DOI: 10.1088/1674-1056/ac0696

High efficient Al: ZnO based bifocus metalens in visible spectrum

Pengdi Wang(王鹏迪) and Xianghua Zeng(曾祥华)†
Chin. Phys. B, 2020, 29 (**10**): 104211. DOI: 10.1088/1674-1056/abab70

Ultraviolet metalens and metalens array of focused vortex beams

Jinping Zhang(张金平)[1,2,†], Yan Wang(王焱)[2,4,†], Huan Yuan(袁欢)[2], Zehao Wang(王泽豪)[1], Yang Deng(邓阳)[1], Chengzhi Huang(黄承志)[3,‡], Jiagui Wu(吴加贵)[1,§], and Junbo Yang(杨俊波)[2,¶]

[1] *School of Physical Science and Technology, Southwest University, Chongqing* 400715, *China*
[2] *Center of Material Science, National University of Defense Technology, Changsha* 410073, *China*
[3] *Key Laboratory of Luminescence Analysis and Molecular Sensing (Southwest University), Ministry of Education, College of Pharmaceutical Sciences, Southwest University, Chongqing* 400715, *China*
[4] *College of Artificial Intelligence, Southwest University, Chongqing* 400715, *China*

(Received 22 June 2022; revised manuscript received 31 August 2022; accepted manuscript online 26 October 2022)

The solar-blind ultraviolet (UV) wavelength is particularly interesting within the range of 200 nm–300 nm. Here, we propose a focusing metalens, focusing vortex beam (VB) metalens and metalens array that specifically work in the UV band to focus a beam or VB. Firstly, a high numerical aperture (NA) focusing metalens working at a wavelength of 214.2 nm was designed, and the NA reached 0.83. The corresponding conversion efficiency of the unit structure reached as high as 94%, and the full width at half maximum was only 117.2 nm. Metalenses with large NA can act as optical tweezers and can be applied to trap ultracold atoms and molecules. Secondly, a focused VB metalens in the wavelength range of 200 nm–300 nm was also designed, which can convert polarized light into a VB and focus the VB simultaneously. Finally, a metalens array was developed to focus VBs with different topological charges on the same focal plane. This series of UV metalenses could be widely used in UV microscopy, photolithography, photonics communication, etc.

Keywords: metalens, metamaterials, ultraviolet (UV), vortex beams

PACS: 42.79.Bh, 78.67.Pt, 42.72.Bj, 42.60.Jf **DOI:** 10.1088/1674-1056/ac9d87

1. Introduction

Optical lenses of ultraviolet (UV) wavelengths have a wide range of applications in lithography, military, and medical fields.[1–4] Traditional UV optical devices process the material into a curved surface to achieve wavefront shaping, which leads to bulky, expensive, and easy aging under UV light.[5–8] The strong absorption of most materials hinders the development of metalenses in UV light. All dielectric materials provide a promising method to control the amplitude, polarization, and phase.[9–16] The application of all dielectric materials to a UV metalens can greatly reduce the size of the device and improve the degree of integration.[17] There are few reports on metalenses in the UV range.[18,19] At present, the function of the metalens in the UV band is relatively single, and the focusing efficiency and polarization conversion efficiency of the unit structure need to be improved urgently. This research proposes a focused metalens and focused vortex beam (VB) metalens that work in the UV band and provide a new solution for improvement of the integration of UV optics.

In recent years, research based on metalenses has developed rapidly. Metalenses have the advantages of small size and easy integration. Yu *et al.* designed a V-shaped metalens with a thickness of only 60 nm, which has the characteristics of double resonance, wide phase coverage, and ultra-thinness, and is expected to replace traditional lenses.[20,21] Using C-shaped resonators with discontinuous phases, Wang *et al.* proposed a planar lens array based on a terahertz metasurface. A metalens with a smaller volume, higher sensitivity, and larger numerical aperture (NA) can be realized.[22] On this basis, research on the expansion of the function of metalenses has also been conducted subsequently. Peng *et al.* designed a chiral metalens that works in the infrared band and can be used as a photon probe to generate a strong pulling force.[23] Bai *et al.* designed a type of dynamic adjustment of the lens array by changing the state of the phase change material to work in the near-infrared band, which can enable the metalens to achieve different optical functions.[24–26] Wang *et al.* designed and prepared an achromatic GaN metalens with a focal length of the order of hundreds of micrometers in the visible light band.[27] Chen *et al.* designed a full-color pixel-level imaging GaN metalens that works in the visible light band, along with beams of different colors that are incident simultaneously to obtain different focal points on the same plane.[28] In recent years, research on metalenses has mainly focused on the visible to infrared wavelengths; however, research on UV metalenses is still in its infancy. However, UV metalenses have extremely important applications in the photolithography, biological, and communication fields.[29–31] The UV lens is a core component of lithography and UV microscopy. It can be also

[†]These authors contributed equally to this work.
[‡]Corresponding author. E-mail: chengzhi@swu.edu.cn
[§]Corresponding author. E-mail: mgh@swu.edu.cn
[¶]Corresponding author. E-mail: yangjunbo@nudt.edu.cn

© 2023 Chinese Physical Society and IOP Publishing Ltd

used to improve the security of communication by using the invisible characteristics of UV in the human eye and to achieve sterilization. This article proposes a metalens that works in the UV band. The unit structure of the metalens in this design satisfies the Pancharatnam–Berry (P–B) phase distribution.[32,33] The metalens can convert circularly polarized light into a VB and focus the VB simultaneously. With the in-depth study of VBs, the carried orbital angular momentum (OAM) has garnered extensive attention in the fields of particle trapping[34] and high-dimensional information processing.[34–37] The combination of a VB and UV metalens could also be used to trap cancer cells, which has great significance in medicine. Traditional VB generators are usually bulky, resulting in low integration of devices. The combination of a metalens and VB generator can significantly reduce the size of the optical components.

UV signals with wavelengths of 200 nm–300 nm only exist in very few cases, such as lightning, and artificial solar blind UV light sources. UV lenses play an important role in nanomanufacturing. First, a single focus lens with a large NA working at 214.5 nm is designed. We choose the incident light of the lens as right circularly polarized (RCP). The single focus lens has a maximum NA of 0.83 and a full width at half maximum (FWHM) of 117.2 nm. The conversion efficiency of the unit structure is 94%, and the polarization conversion efficiency is the ratio of the optical power of the incident RCP light to the outgoing left circularly polarized (LCP) light.[38,39] A single focus metalens with a large NA can be used to manipulate bacteria and viruses in the UV range. Second, metalenses of the single focus focused VB with wavelengths of 214.2 nm, 248.3 nm, 260 nm, and 285.7 nm are designed. Finally, a focused VB metalens array is designed in the UV band, which can focus VBs with different topological charges on the same focal plane. The metalens array can be further extended to several fields, such as wavefront control, communication, and multipixel detector arrays, significantly improving design flexibility and convenience.

2. Structural lens design

A structural diagram of the metalens is shown in Fig. 1(a). When the RCP light is incident on the substrate, the metalens can transform the beam into LCP light. To realize the conversion of polarized light, the unit structure of the lens needs to be filled with the P–B phase, and the nanopillars at any position (x, y) on the lens must satisfy phase equation as follows:

$$\varphi(x,y,f) = \frac{2\pi}{\lambda}\left(f - \sqrt{x^2+y^2+f^2}\right), \tag{1}$$

where f is the focal length of the metalens and λ is the wavelength of the incident light. The unit structure of the metalens is shown in Figs. 1(b)–1(d), with a composition of 400 nm GaN and 100 nm SiO_2. We determine the size of the unit structure by optimizing the parameters of the unit structure: the length of the nanopillar is $l = 0.08$ μm, the width of the nanopillar is $w = 0.05$ μm, and the length and width of the substrate, that is, the period of the unit structure, is $p = 0.15$ μm.

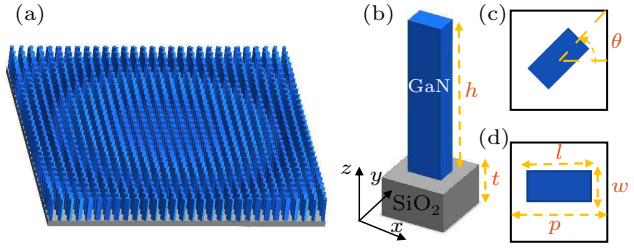


Fig. 1. Schematic of the overall and unit structures of the metalens. (a) Schematic of the overall structure of the metalens; RCP light is incident from the substrate, and the metalens can transform the light beam into LCP light and focus on a specific focal plane. (b) 3D structure diagram of the unit structure, which consists of a SiO_2 substrate and GaN nanopillars. The thickness of the substrate is $t = 100$ nm, and the height of the nanopillars is $h = 400$ nm. (c) and (d) Top views of GaN nanopillars, and θ is the angle formed between the unit structure and the x-axis. The period of the unit structure is $p = 0.15$ μm, and the length $l = 0.08$ μm and width $w = 0.05$ μm of the rectangular nanopillar.

3. Results

CST Studio Suite (Dassault Systèmes Simulia 2016) is used as the simulation software for this design, and in the simulation process, the boundary conditions are set as fully open boundaries. The mesh is set to 5 during simulation. When the wavelength is 214.2 nm, the size of the metalens is 15 μm × 15 μm, and the phase plane is 100 × 100 pixels. The size of a pixel is 0.15 μm × 0.15 μm, which is the same as the size of the unit structure of the metalens. The radius of the designed metalens is 7.5 μm. To obtain a metalens with a smaller FWHM and larger NA, single focus metalenses with focal lengths of 30 μm, 25 μm, 20 μm, 15 μm, 10 μm, and 5 μm were designed and simulated.

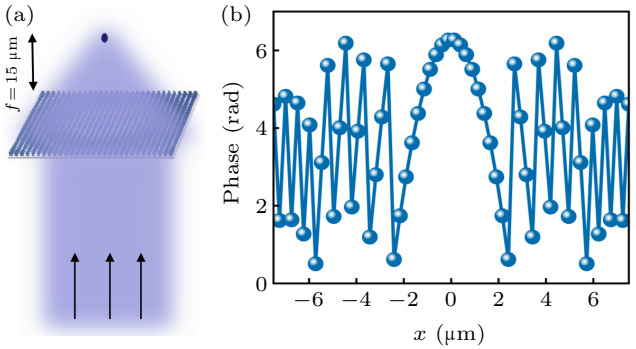


Fig. 2. Design of a single focus metalens with an incident wavelength of 214.2 nm and different focal lengths. (a) Structure layout of the metalens. The radius of the metalens is 7.5 μm and the phase of the unit structure satisfies Eq. (1). (b) Phase distribution of the lens section along the x-axis. The metalens satisfies the phase distribution of 0–2π.

The layout of the unit structure at different positions on the metalens is shown in Fig. 2(a). The phase distribution of the metalens section along the x axis at $y = 0$ is shown in Fig. 2(b). Because the subwavelength structure can only

achieve an approximate continuous phase distribution in a small size range, the phase distribution of the designed plane metalens does not meet the ideal hyperbolic division. The errors in the figure are unavoidable during the design process. A small unit structure can achieve a more ideal phase distribution; however, if the period is excessively small, the coupling between adjacent unit structures cannot be ignored. Therefore, a specific phase continuity must be sacrificed during the design process. The NA and FWHM change as the focal length of the meta lens changes, where NA $= \sin[\tan^{-1}(D/2f)]$, in which D is the diameter of the metalens and f is the focal length. When the focal length is 5 μm, 10 μm, 15 μm, 20 μm, 25 μm, and 30 μm, the FWHM is 117.2 nm, 169.2 nm, 215.9 nm, 340.4 nm, and 427.1 nm, respectively, and the NA is 0.8321, 0.6, 0.4472, 0.3511, 0.2837, and 0.2425, respectively. When the focal point is 5 μm, the FWHM of the focal plane is 117.2 nm, which is slightly smaller than the diffraction limit $\lambda/2\mathrm{NA}$.

Normalized light field distributions of the x–z plane with focal lengths of 30 μm, 25 μm, 20 μm, 15 μm, 10 μm, and 5 μm, are shown in Figs. 3(a)–3(f), respectively. When the focal length is 5 μm, the NA of the lens is 0.83, and the lens can break through the diffraction limit and produce a sharp focus at the far-field diffraction limit. A focal point with an FWHM of 117.2 nm produces a strong optical force, which has great application potential in particle trapping. This provides opportunities in lithography, data recording, and focal plane arrays.

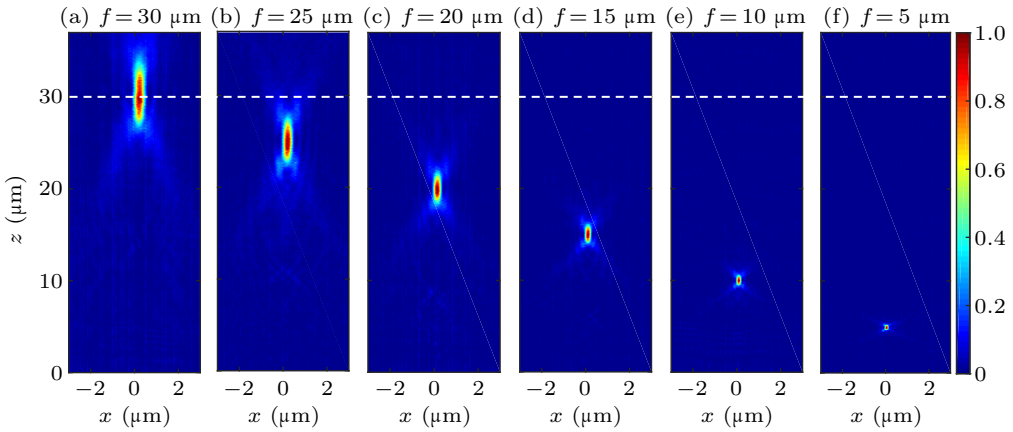


Fig. 3. Light field distribution diagram of the x–z plane of the single focus metalens with different focal lengths. (a)–(f) Normalized light field intensity distribution of the x–z plane with focal lengths of 30 μm, 30 μm, 25 μm, 20 μm, 15 μm, 10 μm, and 5 μm, respectively.

In this design, the rotation angle of the unit structure of the metalens is adjusted using the P–B phase, which make the metalens produce VB carrying OAM,[40–42] and it is necessary to add a spiral phase shift to the plane wave front. The phase distribution of the unit structure must satisfy

$$\varphi'(x,y,f) = \frac{2\pi}{\lambda}\left(f - \sqrt{x^2+y^2+f^2}\right) + l\cdot\arctan(y/x), \quad (2)$$

where (x, y) denotes the coordinate of any point on the plane metalens, f represents the focal length, λ is the wavelength of the incident light, and l is the topological charge of the VB. In this design, the RCP light is used as the incident light. According to the Jones matrix

$$\begin{aligned} E_{\mathrm{out}} &= \alpha \begin{bmatrix} \cos^2\theta & \cos\theta\sin\theta \\ \cos\theta\sin\theta & \sin^2\theta \end{bmatrix} E_{\mathrm{L/R}} \\ &= \alpha \begin{bmatrix} \cos^2\theta & \cos\theta\sin\theta \\ \cos\theta\sin\theta & \sin^2\theta \end{bmatrix} \frac{1}{\sqrt{2}} \begin{bmatrix} 1 \\ \pm \mathrm{i} \end{bmatrix} \\ &= \frac{1}{2\sqrt{2}}\alpha(\cos 2\theta + \mathrm{i}\cdot\sin 2\theta) \begin{bmatrix} 1 \\ \mp \mathrm{i} \end{bmatrix} + \frac{1}{2\sqrt{2}}\alpha \begin{bmatrix} 1 \\ \pm \mathrm{i} \end{bmatrix} \\ &= \frac{1}{2\sqrt{2}}\alpha\, \mathrm{e}^{\mathrm{i}\cdot 2\theta} E_{\mathrm{R/L}} + \frac{1}{2\sqrt{2}}\alpha E_{\mathrm{L/R}}. \end{aligned} \quad (3)$$

Here, E_{out} is the light field distribution of the outgoing light, $E_{\mathrm{L/R}} = 1/\sqrt{2}(e_x \pm \mathrm{i}e_y)$ denotes the polarization state of light, and α is the propagation constant. In fact, the structure designed in this paper is aimed at RCP as the incident light. This method is also applicable to LCP as incident light. When the RCP light is converted into LCP light, the projected reversely polarized light undergoes a geometric phase shift, which is twice the rotation angle of the nanopillar. θ is the angle formed between the unit structure and the x-axis, that is, $\varphi = 2\theta$ is satisfied. Therefore, θ needs to satisfy

$$\theta'(x,y,f) = \frac{\pi}{\lambda}\left(f - \sqrt{x^2+y^2+f^2}\right) + \frac{1}{2}l\cdot\arctan(y/x). \quad (4)$$

A focused VB metalens with an incident wavelength of 214.2 nm and a vortex topological charge of 2 is designed. This metalens is denoted by $\mathrm{V}_{214.2}$ hereon. The phase distribution of the metalens satisfies Eq. (2) and the overall arrangement of the plane lens is shown in Fig. 4(a). The unit structure still uses 400 nm GaN placed on a 100 nm SiO_2 substrate. The size of the focused VB metalens is 15 μm × 15 μm, the phase plane of the lens is 100 × 100 pixels, the radius of the designed metalens is $R = 7.5$ μm, and the focal length is set to 15 μm. Figure 4(b) is a diagram of light field intensity in the x–z direction and intensity distributions in the focal plane, as measured for metalens $\mathrm{V}_{214.2}$. The focal length obtained by

the simulation calculation is slightly smaller than the actual focal length. The reason for this result may be errors in the simulation process. Figure 4(b) shows that the FWHM in the x and y directions is 654.2 nm.

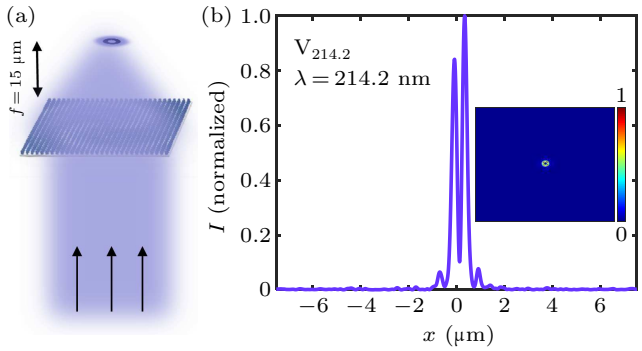


Fig. 4. Design of a metalens for a focused VB with a wavelength of 214.2 nm and a topological charge of 2. (a) Structure diagram of the focused VB metalens, the overall arrangement of the unit structure satisfies Eq. (2). (b) Cross-focus cuts and intensity distributions in the focal plane, as measured for metalenses $V_{214.2}$.

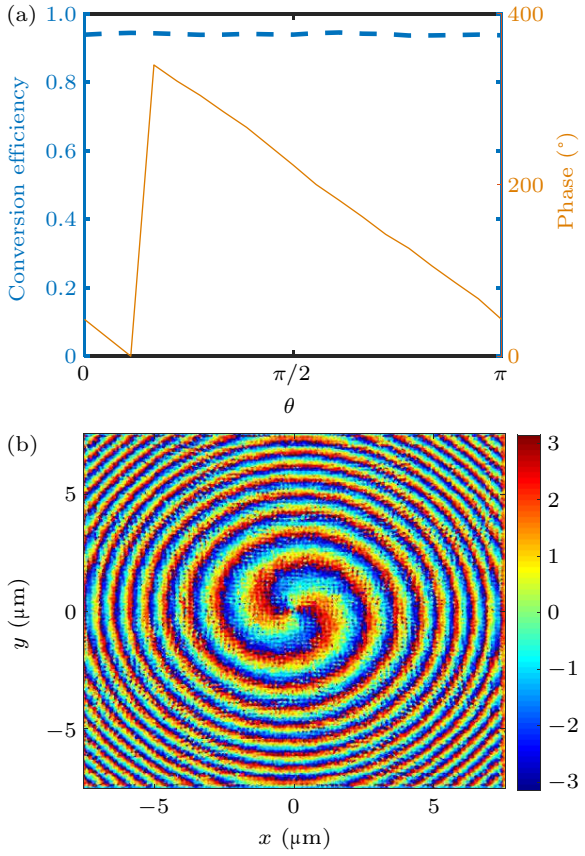


Fig. 5. Analysis of the focusing effect of a focused VB metalens with an incident light wavelength of 214.2 nm and a vortex topological charge of 2. (a) Relationship between the conversion efficiency of the unit structure and the phase distribution with the rotation angle of the nanopillars. (b) Phase distribution of the metalens; the phase distribution of the metalens satisfies 0–2π.

The simulation result of the $V_{214.2}$ metalens is shown in Fig. 5. Figure 5(a) shows the conversion efficiency and phase distribution of the unit structure as a function of the rotation angle of the nanopillars. The conversion efficiency of the unit structure is 94%. The unit structure of the metalens can make the phase shift meet the phase modulation of 0–2π. Most of the incident RCP light is converted into VB carrying OAM and focuses on the focal plane 15 μm from the metalens. Figure 5(b) shows the phase distribution of the $V_{214.2}$ metalens. The metalens can convert RCP light into a VB and focus the VB simultaneously. The beam can be focused into a donut-shaped annular aperture on a specific focal plane.

Focused VB metalenses with a topological charge of 2 and incident wavelengths of 248.3 nm, 260 nm, and 285.7 nm are designed. Hereon, they are represented by $V_{248.3}$, V_{260}, and $V_{285.7}$, respectively. Figure 6 shows the simulation results of the $V_{248.3}$, V_{260}, and $V_{285.7}$ metalenses. The average conversion efficiencies of the cell structures at the three wavelengths are 93%, 76%, and 69%, respectively. Figures 6(a)–6(c) show light field intensity in the x–z direction and intensity distributions in the focal plane, as measured for metalenses $V_{248.3}$, V_{260}, and $V_{285.7}$, respectively. The FWHM values are 914 nm, 928.6 nm, and 894 nm, respectively. Each of the three metalenses can focus the VB on a specific focal plane, forming a donut-shaped annular aperture. Figures 6(d)–6(f) show the phase distributions of the metalenses at the three wavelengths. It can be seen from the figure that the phase of the metalens satisfies the phase distribution of 0–2π. Figures 6(g)–6(i) are the intensity distribution diagrams of the three metalenses in the x–z plane, and the focal lengths obtained by simulation are 14.85 μm, 14.73 μm, and 14.5 μm, respectively. The focal length of the focused VB metalens decreases as the incident wavelength increases. The design of a focused VB metal is realized in the UV range. The lens can be widely used in particle manipulation and cell and virus manipulation.

This study also designs a metalens array of focused VB with wavelengths of 214.2 nm, 248.3 nm, 260 nm, and 285.7 nm, which can focus VBs of different topological charges on the same plane at different focal points. The upper left $l = -1$, upper right $l = 1$, lower left $l = -2$, and lower right $l = 2$ of the metalens array. The structure diagram of the focused VB metalens array is shown in Fig. 7(a). Figure 7(b) shows the phase distribution of the metalens array. It can be seen from the figure that the phase of the lens satisfies the phase distribution of 0–2π. The phase plane is set as 100×100 pixels, the focal length as 15 μm, and the lens radius as 7.5 μm. Figure 8 shows the simulation results of focusing the VB metalens array with different topological charges. Figures 8(a)–8(d) show the diagram of the light field intensity in the x–y direction at the focal plane when the wavelengths are 214.2 nm, 248.3 nm, 260 nm, and 285.7 nm, respectively. The metalens arrays at three wavelengths can convert RCP light into VB and focus the VB simultaneously. The array can focus the VB with different OAM on different focal points on the same plane, forming four donut-shaped annular spots at the focal point.

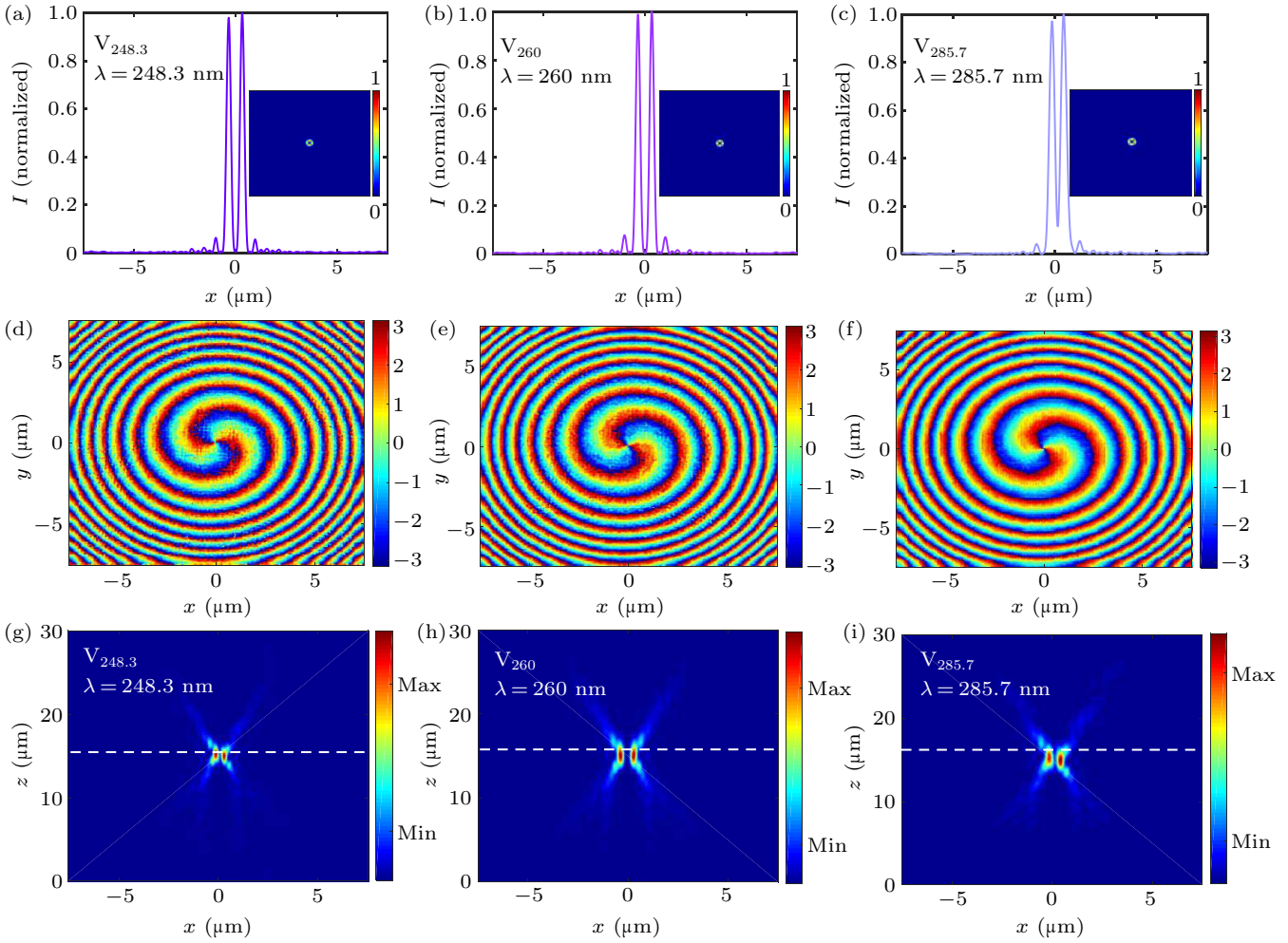


Fig. 6. Focusing effect of the $V_{248.3}$, V_{260}, and $V_{285.7}$ metalenses. (a)–(c) Cross-focus cuts and intensity distributions in the focal plane, as measured for metalenses $V_{248.3}$, V_{260}, and $V_{285.7}$. (d)–(f) Phase distribution diagram of the $V_{248.3}$, V_{260}, and $V_{285.7}$ metalenses, and phase distribution at all three wavelengths satisfying 0–2π. (g)–(i) Metalens x–z plane intensity distribution diagram of the $V_{248.3}$, V_{260}, and $V_{285.7}$ metalenses.

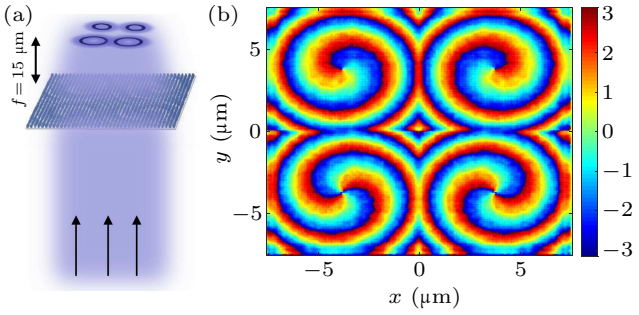


Fig. 7. Design of a metalens array for focusing a VB with different OAM. (a) Structure diagram of the focused VB metalens array. Topological charges of the four lenses in the array are upper left $l = -1$, upper right $l = 1$, lower left $l = -2$, lower right $l = 2$, and the radius of the lens is 7.5 μm. (b) Phase distribution diagram of the lens array; the phase distributions of the four lenses in the array all satisfy 0–2π.

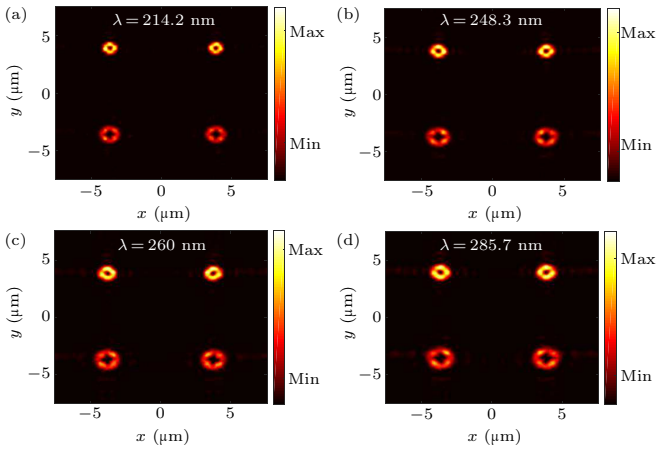


Fig. 8. Design of a metalens array with different wavelengths in the UV band. (a)–(d) Light field intensity in the x–y direction at the focal plane when the wavelengths are 214.2 nm, 248.3 nm, 260 nm, and 285.7 nm, respectively. The lens arrays of four wavelengths can focus the VB with different OAM on the same focal plane.

Based on the 2×2 array design, we also design a 3×3 lens array that can focus the VB with different OAM on the same focal plane. The structure diagram of the focused VB metalens array is shown in Fig. 9(a). The phase plane is set as 120×120 pixels, the focal length as 10 μm, and the radius of the lens as 9 μm. The metalens can focus the VB with vortex topological charges of $l = 1$, $l = 2$, and $l = 3$ on the focal plane at a distance of 10 μm from the lens array. Figure 9(b) shows the phase distribution of the metalens array. It can be seen from the figure that the phase of the lens satisfies the phase distribution of 0–2π. Figures 10(a)–10(d) show the light field intensity in the x–y direction at the focal plane when the wavelengths of the lens array are 214.2 nm,

248.3 nm, 260 nm, and 285.7 nm, respectively. The lens arrays at the four wavelengths can focus the VB with different OAM into a donut-shaped annular spot. The designed lens array can be further extended to several fields, such as wavefront control, communication, and multi-pixel detector arrays.

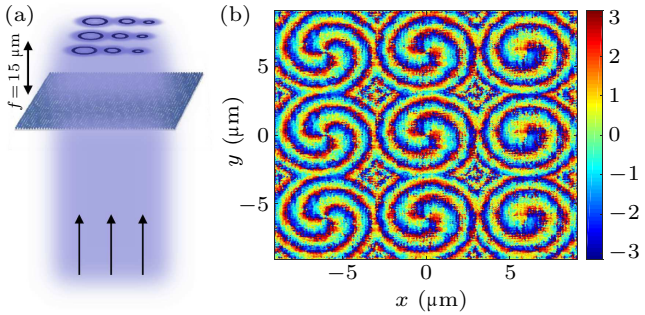


Fig. 9. Design of 3×3 metalens array for focusing a VB with different OAM. The topological charge in the lens array is set as $l = 3$ in the left column, $l = 2$ in the middle column, and $l = 1$ in the right column. (a) Structure diagram of the focused VB metalens array; the radius of the lens is 9 μm. (b) Phase distribution diagram of the lens array; the phase distributions of the nine lenses in the array all satisfy 0–2π.

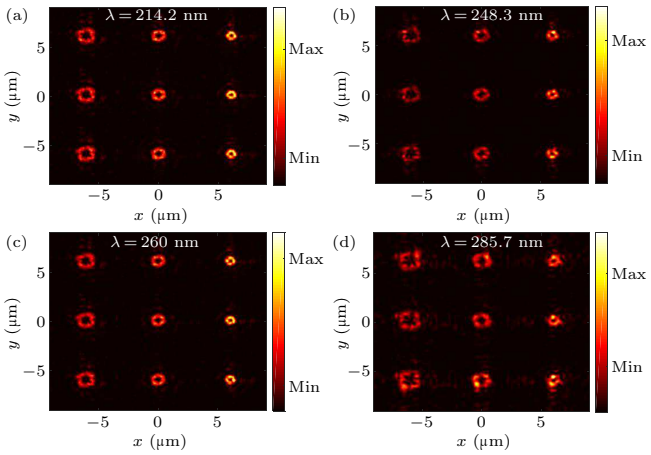


Fig. 10. Design of a 3×3 metalens array for focusing a VB with different OAM. (a)–(d) The light field intensity in the x–y direction at the focal plane when the wavelengths are 214.2 nm, 248.3 nm, 260 nm, and 285.7 nm, respectively. The four-wavelength 3×3 lens array can focus the VB with different OAM on the same focal plane.

4. Discussion

In this study, GaN material is optimized used to realize the UV metalens, with a band gap of about 3.4 eV (equal to a wavelength of 364.67 nm) and a good transparent window of 100 nm–600 nm. Our GaN-based metalens and lens array possess some unique features compared with other UV metalenses published in recent years. The results are shown in Table 1. When the wavelength is 250 nm, the FWHM of the UV metalens made of Si_3N_4 is 206 nm,[17] the NA is 0.75, and the conversion efficiency is 96%, which is slightly higher than the conversion efficiency of the other materials. When the wavelength is 260 nm, the UV metalens prepared by MgO has an FWHM of 182 nm and a NA of 0.8.[43] When the wavelength is 375 nm, the metalens is composed of AlN,[39] for which the FWHM is about 620 nm and the NA is 0.196. In contrast, we choose GaN in this study. The corresponding FWHM of the metalens is optimized to be as small as 117 nm and the NA is as high as 0.83. Compared with the other results in Table 1, our FWHM value is the smallest, and simultaneously, our NA value is the highest. This lens focal spot with large NA and small FWHM is highly beneficial for the large gradient force generation required in the optical tweezers field,[44,45] such as for trapping cells and small particles. Considering our results of about 100 nm FWHM and 0.83 NA, it is possible to trap COVID-19 viruses and other nanoparticles. The diameter of the COVID-19 virus is usually 60 nm–140 nm, and a metalens device with a smaller FWHM is conducive to better directional sterilization. In addition, metalenses with large NA can be used as light cameras and can be applied to trap ultracold atoms and molecules.

Table 1. Performance comparison of different materials of metalenses in the UV band.

Material	Wavelength	FWHM	NA	Conversion efficiency	Whether it focuses the VB
Si_3N_4[17]	250 nm	206 nm	0.75	96%	no
MgO[43]	260 nm	182 nm	0.8	94%	no
AlN[39]	375 nm	620 nm	0.196	79.46%	no
GaN	214.2 nm	117 nm	0.83	94%	yes

The main limitation of metalens fabrication is the high aspect ratio of the cell structure.[46] Here, our cell structure parameters of the metalens are $l = 80$ nm, $w = 50$ nm, and $h = 400$ nm. Therefore, the aspect ratio is 8, which is lower than that in Ref. [46]. Therefore, our cell structure is basically easier than that in Ref. [46] for fabrication. Additionally, considering that Refs. [47–49] realized small-size metasurface processing, our UV metalens cell structures could also use photolithography for possible scalable fabrication.

5. Conclusion

In this article, we propose both a focusing metalens and a focusing VB metalens that work in the UV band. The phase distribution of the metalens unit structure satisfies the P–B phase. The polarization conversion efficiency of the focusing lens in the UV band reaches 94%. When the focal length is 5 μm, the NA of the lens is 0.83, and the FWHM size of the focal point is only 117.2 nm, which can produce a strong light force for future nanoparticle trapping. Next, we realize a focused VB metalens that works in the UV band by adding a helical phase shift to the plane wavefront. Furthermore, 2×2 and 3×3 VB metalens arrays are also designed, which can focus the VB with different OAM on the same focal plane. The focusing metalens, focusing VB metalens and metalens array in the UV band could have broad applications in wavefront control, optical manipulation, imaging, target guidance and other fields.

Acknowledgments

Project supported by the National Natural Science Foundation of China (Grant Nos. 60907003, 61805278, 61875168, and 22134005), Chongqing Science Funds for Distinguished Young Scientists (Grant No. cstc2021jcyj-jqX0027), Innovation Research 2035 Pilot Plan of Southwest University (Grant No. SWU-XDPY22012), China Postdoctoral Science Foundation (Grant No. 2018M633704), Innovation Support Program for Overseas Students in Chongqing (Grant No. cx2021008), Foundation of NUDT (Grant Nos. JC13-02-13 and ZK17-03-01), Hunan Provincial Natural Science Foundation of China (Grant No. 13JJ3001), Program for New Century Excellent Talents in University (Grant No. NCET-12-0142), and Chongqing Talents Program for Outstanding Scientists (Grant No. cstc2021ycjh-bgzxm0178).

References

[1] Brizuela F, Wang Y, Brewer C, Pedaci F, Chao W, Anderson E, Liu Y, Goldberg K A, Naulleau P, Wachulak P, Marconi M C, Attwood D T, Rocca J J and Menoni C S 2009 *Opt. Lett.* **34** 271
[2] Harata A, Matuda T and Hirashima S 2007 *Jpn. J. Appl. Phys.* **46** 4561
[3] Hirai Y, Inamoto Y, Sugano K, Tsuchiya T and Tabata O 2006 *Journal of Micromechanics and Microengineering* **17** 199
[4] Takahashi H, Heo Y J, Arakawa N, Kan T, Matsumoto K, Kawano R and Shimoyama I 2016 *Microsystems and Nanoengineering* **2** 16049
[5] Bendickson J M, Glytsis E N and Gaylord T K 1999 *JOSA A* **16** 113
[6] Chen W T, Zhu A Y, Khorasaninejad M, Shi Z, Sanjeev V and Capasso F 2017 *Nano Lett.* **17** 3188
[7] Fujita T, Nishihara H and Koyama J 1982 *Opt. Lett.* **7** 578
[8] Ye J S, Zhang Y and Hane K 2009 *Opt. Express* **17** 7348
[9] Ahmadivand A, Gerislioglu B and Ramezani Z 2019 *Nanoscale* **11** 8091
[10] Huang B, Bai W, Jia H, Han J, Guo P, Wu J and Yang J 2020 *Results in Physics* **17** 103085
[11] Jiang Q, Bao Y, Lin F, Zhu X, Zhang S and Fang Z 2018 *Adv. Funct. Mater.* **28** 1705503
[12] Khorasaninejad M, Shi Z, Zhu A Y, Chen W T, Sanjeev V, Zaidi A and Capasso F 2017 *Nano Lett.* **17** 1819
[13] Li B, Piyawattanametha W and Qiu Z 2019 *Micromachines* **10** 310
[14] Li G, Zhang S and Zentgraf T 2017 *Nat. Rev. Mater.* **2** 17010
[15] Liang Y, Liu H, Wang F, Meng H, Guo J, Li J and Wei Z 2018 *Nanomaterials* **8** 288
[16] Mueller J B, Rubin N A, Devlin R C, Groever B and Capasso F 2017 *Phys. Rev. Lett.* **118** 113901
[17] Kanwal S, Wen J, Yu B, Kumar D, Chen X, Kang Y, Bai C and Zhang D 2020 *Nanomaterials* **10** 490
[18] Guo L, Hu Z, Wan R, Long L, Li T, Yan J, Lin Y, Zhang L, Zhu W and Wang L 2019 *Nanophotonics* **8** 171
[19] Kanwal S, Wen J, Yu B, Chen X, Kumar D, Kang Y, Bai C, Ubaid S and Zhang D 2020 *Nanomaterials* **10** 1439
[20] Yu N, Aieta F, Genevet P, Kats M A, Gaburro Z and Capasso F 2012 *Nano Lett.* **12** 6328
[21] Yu N, Genevet P, Kats M A, Aieta F, Tetienne J P, Capasso F and Gaburro Z 2011 *Science* **334** 333
[22] Li Q T, Dong F, Wang B, Gan F, Chen J, Song Z, Xu L, Chu W, Xiao Y F and Gong Q 2016 *Opt. Express* **24** 16309
[23] Arbabi A, Horie Y, Ball A J, Bagheri M and Faraon A 2015 *Nat. Commun.* **6** 7069
[24] Lin D, Holsteen A L, Maguid E, Wetzstein G, Kik P G, Hasman E and Brongersma M L 2016 *Nano Lett.* **16** 7671
[25] Khorasaninejad M, Chen W T, Devlin R C, Oh J, Zhu A Y and Capasso F 2016 *Science* **352** 1190
[26] Khorasaninejad M, Zhu A Y, Roques-Carmes C, Chen W T, Oh J, Mishra I, Devlin R C and Capasso F 2016 *Nano Lett.* **16** 7229
[27] Lalanne P, Astilean S, Chavel P, Cambril E and Launois H 1998 *Opt. Lett.* **23** 1081
[28] Chen B H, Wu P C, Su V C, Lai Y C, Chu C H, Lee I C, Chen J W, Chen Y H, Lan Y C and Kuan C H 2017 *Nano Lett.* **17** 6345
[29] Brizuela F, Wang Y, Brewer C A, Pedaci F, Chao W, Anderson E H, Liu Y, Goldberg K A, Naulleau P, Wachulak P, Marconi M C, Attwood D T, Rocca J J and Menoni C S 2009 *Opt. Lett.* **34** 271
[30] Takahashi H, Jung Heo Y, Arakawa N, Kan T, Matsumoto K, Kawano R and S himoyama I 2016 *Microsystems Nanoengineering* **2** 16049
[31] Hirai Y, Inamoto Y, Sugano K, Tsuchiya T and Tabata O 2007 *Journal of Micromechanics and Microengineering* **17** 199
[32] Wang S, Wu P C, Su V C, Lai Y C, Chen M K, Kuo H Y, Chen B H, Chen Y H, Huang T T and Wang J H 2018 *Nat. Nanotechnol.* **13** 227
[33] Lin R and Li X 2019 *Opt. Lett.* **44** 2819
[34] Simpson N, Allen L and Padgett M 1996 *J. Mod. Opt.* **43** 2485
[35] Gibson G, Courtial J, Padgett M J, Vasnetsov M, Pas'ko V, Barnett S M and Franke-Arnold S 2004 *Opt. Express* **12** 5448
[36] Grier D G 2003 *Nature* **424** 810
[37] Mair A, Vaziri A, Weihs G and Zeilinger A 2001 *Nature* **412** 313
[38] Vallone G, D'Ambrosio V, Sponselli A, Slussarenko S, Marrucci L, Sciarrino F and Villoresi P 2014 *Phys. Rev. Lett.* **113** 060503
[39] Guo L, Xu S, Wan R, Li T, Xiong L, Wang L and Zhu W 2018 *Journal of Nanophotonics* **12** 043513
[40] Tian S, Guo H, Hu J and Zhuang S 2019 *Opt. Express* **27** 680
[41] Ma Y, Rui G, Gu B and Cui Y 2017 *Scientific Reports* **7** 1
[42] Zhang K, Yuan Y, Zhang D, Ding X, Ratni B, Burokur S N, Lu M, Tang K and Wu Q 2018 *Opt. Express* **26** 1351
[43] Ali F and Aksu S 2021 *Scientific Reports* **11** 1
[44] Chantakit T, Schlickriede C, Sain B, Meyer F, Weiss T, Chattham N and Zentgraf T 2020 *Photonics Research* **8** 1435
[45] Ma L, Guan J, Wang Y, Chen C, Zhang J, Lin J, Tan J and Jin P 2020 *Nanophotonics* **9** 841
[46] Zhang C, Divitt S, Fan Q, Zhu W, Agrawal A, Lu Y, Xu T and Lezec H J 2020 *Light Science Applications* **9** 55
[47] Deng Y, Wang X, Gong Z, Dong K, Lou S, Pegard N, Tom K B, Yang F, You Z, Waller L and Yao J 2020 *Adv. Mater.* **30** e1802632
[48] Huang K, Deng J, Leong H S, Yap S L K, Yang R B, Teng J and Liu H 2019 *Laser and Photonics Reviews* **13** 1800289
[49] Tseng M L, Semmlinger M, Zhang M, Arndt C, Huang T T, Yang J, Kuo H Y, Su V C, Chen M K, Chu C H, Cerjan B, Tsai D P, Nordlander P and Halas N J 2022 *Sci. Adv.* **8** eabn5644